ligand spin density favors antiferromagnetic coupling in these intermediates (*16*).
16. M. T. Green, *J. Am. Chem. Soc.* **123**, 9218 (2001).
17. With the use of Gaussian 98, we performed density functional calculations (B3LYP/6-311G) on a ferryl porphine with a methyl thiolate ligand and the appropriate distal ligand.
18. All XAS experiments were performed at the Stanford Synchrotron Radiation Laboratory (SSRL) on beamline 7-3 at $T \approx 10$ K. The data were collected with the use of a Si (220) phi = 0° double crystal monochromator detuned 50% at 8131 eV for harmonic rejection. CPO-II, CPO, HRP-II, and HRP-I data sets were collected with a Canberra (Canaberra Industries, Meriden, CT) 30-element Ge detector. The P450 data sets were collected with a Canberra 13-element Ge detector. All XAS experiments were done in fluorescence mode. The program XAS COLLECT was used for data acquisition. XAS data were analyzed with the curve-fitting program EXAFSPAK (available at http://ssrl.slac.stanford.edu/exafspak.html) with the use of ab initio phases and amplitudes generated with the program FEFF version 8.x39, available at http://leonardo.phys.washington.edu/feff (*19*). Data were collected to $k = 16$ Å^{-1}, where k is photoelectron wave vector, for all samples. To minimize photoreduction, multiple samples were used to collect data for the high-valent systems. Data sets contained the following numbers of total scans: CPO-II (for pH = 5.5, 70, and for pH = 6.7, 164), CPO (190), HRP-II (133), HRP-I (60), HS-P450 (123), and LS-P450 (158). The following (approximate) x-ray absorption edge shifts (in eV) were observed during data collection: CPO-II (0.5), CPO (0.2), HRP-II (0.4), HRP-I (0.3), HS-P450 (0.2), and LS-P450 (0.2). CPO-II showed the largest shifts during data collection, but smaller data sets (20 total scans, two samples and 10 scans each) with smaller edge shifts (≈0.2 eV) resulted in indistinguishable fits. Thus photoreduction appears to be minimal. Data sets were fit over the region of k from 1 to 16 Å^{-1}. (An exception was the pH = 6.7 CPO-II sample, which was fit over the range of k from 1 to 15 Å^{-1} as a result of lower signal to noise.) In some cases a monochromator glitch at $k \approx 11.5$ Å^{-1} was removed by fitting a cubic polynomial to the raw data, but no smoothing, Fourier filtering, or related manipulations were performed. Fit parameters were unaffected by glitch removal. Fits included first and second shell atoms and one multiple scattering component. Only the first shell components are shown. In all cases the second shell was composed of α- and meso-carbons and the Fe-C_α-N-Fe multiple scattering paths (N values of 8, 4, and 16, respectively). The Debye-Waller factors, σ^2, of Fe-C_α-N-Fe multiple scattering paths and the α carbons were constrained to be in a ratio of 1.52 (±0.01) but were otherwise allowed to vary freely. All other Debye-Waller factors were treated as free parameters. The scale factor, S_0, was set to 0.9. CPO was obtained from *Caldariomyces fumago* and purified according to known procedures. CPO-II samples (≈2 mM in 0.3 M potassium phosphate) were prepared at pH values of 5.5 and 6.7 by mixing stock solutions of peracetic acid and ascorbate with ferric enzyme (purity ratio, Rz > 1.4). This mixture was quickly transferred to an XAS sample holder and rapidly frozen in a bath of cold isopentane. A visible absorption spectrum of an unused portion of the reaction mixture was taken after the XAS sample was frozen. This spectrum revealed that the CPO-II samples used for XAS measurements were greater than 90% CPO-II at the time of freezing. Cytochrome $P450_{cam}$ was expressed in *Escherichia coli* and purified by standard procedures. The camphor-bound (HS) sample was ≈ 4 mM in P450 (Rz = 1.56). The substrate-free (LS) sample was ≈2 mM (Rz = 1.35). Both samples were in potassium phosphate buffer (40 mM and pH = 7.5). The HS sample also contained 100 mM KCl and 10 mM camphor. Horseradish peroxidase (Sigma) was purified according to standard methods. HRP (Rz ≈ 3.2) and stock solutions of peracetic acid and ascorbate were used to generate HRP-II and HRP-I according to known procedures. XAS samples (≈ 2 mM in 0.3 M potassium phosphate) were at pH = 6.
19. A. L. Ankudinov, B. Ravel, J. J. Rehr, S. D. Conradson, *Phys. Rev. B* **58**, 7565 (1998).
20. J. E. Penner-Hahn *et al.*, *J. Am. Chem. Soc.* **108**, 7819 (1986).
21. T. Wolter *et al.*, *J. Inorg. Biochem.* **78**, 117 (2000).
22. With the use of a stopped flow apparatus, we examined the visible absorption spectrum of CPO-II under steady state conditions (using peracetic acid and ascorbate) at pH values of 3.5 and 6.9. No difference in the absorption maxima of the Soret (437 nm) or Q bands (541 and 571 nm) of CPO-II was observed. Minor variations in the bluest peak (372 nm) are attributable to changes in the relative steady state concentrations of compounds I and II as a function of pH (*23*). CPO-I absorbs at 367 and 688 nm. CPO undergoes an irreversible alkaline transition above pH = 7.
23. A. M. Lambeir, H. B. Dunford, M. A. Pickard, *Eur. J. Biochem.* **163**, 123 (1987).
24. M. Chance, L. Powers, T. Poulos, B. Chance, *Biochemistry* **25**, 1266 (1986).
25. A. J. Sitter, C. M. Reczek, J. Terner, *J. Biol. Chem.* **260**, 7515 (1985).
26. C. M. Reczek, A. J. Sitter, J. Terner, *J. Mol. Struct.* **214**, 27 (1989).
27. J. R. Kincaid, Y. Zheng, J. Al-Mustafa, K. Czarnecki, *J. Biol. Chem.* **271**, 28805 (1996).
28. B. Chance *et al.*, *Arch. Biochem. Biophys.* **235**, 596 (1984).
29. Recent crystallographic investigations indicate that other protein ferryl species may be protonated as well. Reported Fe-O bond lengths in HRP-II, myoglobin-II (Mb-II), and cytochrome c peroxidase–I (CCP-I) are 1.8, 1.92, and 1.87 Å, respectively (*30*–*32*). However, it is difficult to reconcile the observed ferryl stretching frequencies with the long Fe-O bonds found in these crystal structures. Much weaker stretches would be expected for these intermediates, if their Fe-O bonds were truly 8, 16, and 13% longer than that of HRP-I.
30. G. I. Berglund *et al.*, *Nature* **417**, 463 (2002).
31. H.-P. Hersleth, B. Dalhus, C. H. Görbitz, K. K. Andersson, *J. Biol. Inorg. Chem.* **7**, 299 (2002).
32. C. A. Bonagura *et al.*, *Biochemistry* **42**, 5600 (2003).
33. F. van Rantwijk, R. A. Sheldon, *Curr. Opin. Biotechnol.* **11**, 554 (2000).
34. H. B. Dunford, *Heme Peroxidases* (Wiley-VCH, New York, 1999).
35. M. P. J. van Deurzen, F. van Rantwijk, R. A. Sheldon, *Tetrahedron* **53**, 13183 (1997).
36. J. M. Mayer, *Acc. Chem. Res.* **31**, 441 (1998).
37. F. G. Bordwell, J.-P. Cheng, G.-Z. Ji, A. V. Satish, X. Zhang, *J. Am. Chem. Soc.* **113**, 9790 (1991).
38. Y. Hayashi, I. Yamazaki, *J. Biol. Chem.* **254**, 9101 (1979).
39. CPO-I oxidizes chloride at pH = 3 (*40*). It must have a two-electron reduction potential in excess of 1.18 V at pH = 6. The two-electron reduction potential of peroxide (1.41 V at pH = 6) provides an upper limit for the CPO-I reduction potential.
40. R. D. Libby, J. A. Thomas, L. W. Kaiser, L. P. Hager, *J. Biol. Chem.* **257**, 5030 (1982).
41. We thank M. Bollinger, I. Dmochowski, J. Labinger, M. Machczynski, M. McGuirl, A. Tezcan, and J. Winkler for helpful discussions; G. George, I. Pickering, M. Latimer, B. Butler, A. Soo Hoo, S. Debeer George, D. Durkin, and other SSRL staff members for assistance with XAS measurements; and L. Hager for a CPO sample used in the initial experiments. Supported by NIH (GM26730 to J.H.D. and DK19038 to H.B.G.), NSF, and the Arnold and Mabel Beckman Foundation.

18 February 2004; accepted 21 April 2004

Iron Isotope Fractionation and the Oxygen Fugacity of the Mantle

Helen M. Williams,[1]* Catherine A. McCammon,[2] Anne H. Peslier,[3] Alex N. Halliday,[1] Nadya Teutsch,[1] Sylvain Levasseur,[1] Jean-Pierre Burg[1]

The oxygen fugacity of the mantle exerts a fundamental influence on mantle melting, volatile speciation, and the development of the atmosphere. However, its evolution through time is poorly understood. Changes in mantle oxidation state should be reflected in the Fe^{3+}/Fe^{2+} of mantle minerals, and hence in stable iron isotope fractionation. Here it is shown that there are substantial (1.7 per mil) systematic variations in the iron isotope compositions ($\delta^{57/54}$Fe) of mantle spinels. Spinel $\delta^{57/54}$Fe values correlate with relative oxygen fugacity, $Fe^{3+}/\Sigma Fe$, and chromium number, and provide a proxy of changes in mantle oxidation state, melting, and volatile recycling.

The redox evolution of the mantle is poorly constrained but is critical to understanding mantle melting, core-mantle exchange, volatile speciation, and the evolution of the mantle and atmosphere. The mantle's oxidation state is quantified in terms of relative oxygen fugacity ($\Delta\log f_{O_2}$). There are only a few good ways of determining $\Delta\log f_{O_2}$ in modern and ancient igneous rocks. In pristine samples, $\Delta\log f_{O_2}$ may be determined using mineral Fe^{3+}/Fe^{2+} equilibria; in altered Achaean and Proterozoic rocks, $\Delta\log f_{O_2}$ is estimated using bulk sample and spinel Cr and V abundances (*1*, *2*).

Iron isotope data for mafic minerals provide evidence of substantial fractionation in the mantle (*3*). According to theory, the heavier isotopes will be incorporated preferentially in bonds where Fe(III) predominates over Fe(II) (*4*, *5*). Therefore, iron isotopes have potential use as tracers of changes in iron oxidation state and mantle $\Delta\log f_{O_2}$.

[1]Department of Earth Sciences, ETH-Zürich, Sonneggstrasse 5, CH-8092 Switzerland. [2]Bayerisches Geoinstitut, Universität Bayreuth, D-95440 Bayreuth, Germany. [3]Texas Center for Superconductivity, University of Houston, Houston, TX 77204, USA.

*To whom correspondence should be addressed. E-mail: williams@erdw.ethz.ch

Spinels are ideal for investigating the role of oxidation in fractionating Fe isotopes in the mantle because they accommodate substantial Fe^{3+} and are sensitive indicators of $\Delta\log f_{O_2}$ (*6*–*9*). Using multiple collector inductively coupled plasma mass spectrometry (MC-ICPMS) and Mössbauer spectroscopy, we measured the iron isotopic compositions and $Fe^{3+}/\Sigma Fe$ of spinels from pristine mantle xenoliths and ultramafic massif samples that are in textural equilibrium. We chose a range of well-characterized samples from fore-arc, continental margin, and intraplate (garnet and spinel-facies) settings (*10*–*12*) to evaluate the effects of mineralogy, melting, and mantle oxidation state on iron isotope fractionation.

Correlations were found between $\delta^{57/54}Fe$ and $\Delta\log f_{O_2}$, $Fe^{3+}/\Sigma Fe$, and Cr number in spinel grains (Fig. 1, A to C), providing evidence for a relation between spinel $\delta^{57/54}Fe$, mantle oxidation state, and melt depletion. This is consistent with sample mineralogy: The Kohistan arc dunites have the lightest $\delta^{57/54}Fe$ and highest $\Delta\log f_{O_2}$, $Fe^{3+}/\Sigma Fe$, and Cr number values; the spinel lherzolites are intermediate in these parameters; and the Cameroon Line garnet websterites have the heaviest $\delta^{57/54}Fe$ and lowest $\Delta\log f_{O_2}$, $Fe^{3+}/\Sigma Fe$, and Cr number values. The $\Delta\log f_{O_2}$ values of the arc rocks, except the Ventura-Esperitu peridotites, agree with $\Delta\log f_{O_2}$ estimates for subarc mantle (*7*, *12*, *13*). The intraplate spinel peridotites have $\Delta\log f_{O_2}$ values within the range previously determined for such rocks (*7*). The $\Delta\log f_{O_2}$ values of the garnet websterites are lower than those of all the other (spinel facies) samples and are similar to those calculated for cratonic garnet peridotites (*14*).

The inverse relation between spinel $\delta^{57/54}Fe$ and $Fe^{3+}/\Sigma Fe$ contrasts with experimental (low-temperature) and theoretical (high-temperature) studies of equilibrium iron isotope fractionation, which predict that species in which Fe(III) predominates will have heavier isotope compositions (*4*, *5*). Comparisons with these studies are not straightforward, because it cannot be assumed that all samples behaved as closed systems with respect to iron or that they equilibrated under identical conditions. Spinel $\delta^{57/54}Fe$ values broadly reflect those of the bulk samples (Table 1), suggesting that spinel $\delta^{57/54}Fe$ reflects open-system processes causing iron isotope variation at the bulk-rock scale. Melt extraction is an open-system process that can explain the large variations in bulk rock and spinel $\delta^{57/54}Fe$ values, because spinel $\delta^{57/54}Fe$ is correlated with Cr number (Fig. 1C), an index of depletion and melt extraction in spinel-facies mantle rocks (*15*).

For the arc samples, the correlations of $\delta^{57/54}Fe$ with $\Delta\log f_{O_2}$, $Fe^{3+}/\Sigma Fe$, and Cr number provide evidence that iron isotope fractionation relates to melting and fluxing of the subarc mantle by hydrous fluids/melts originating from the slab. These agents oxidize and lower the solidus of the subarc mantle, permitting large degrees of melt extraction. Iron isotope fractionation between melt and residue may change with the bonding environment and oxidation state of iron. Isotopically heavy iron could be preferentially incorporated into arc magmas relative to their source, leaving an isotopically light residue. Whether this is related to the greater incompatibility of Fe^{3+}, relative to Fe^{2+}, during melting is unclear, because the behavior of ferric iron during melting in the spinel facies is poorly understood. Although it has been suggested (*16*) that Fe^{3+} is more incompatible than Fe^{2+}, this has not been experimentally corroborated. In fact, the oxidized nature of the subarc mantle samples and their high spinel $Fe^{3+}/\Sigma Fe$ values provide evidence that considerable ferric iron, hosted in spinel, is retained in the subarc mantle during partial melting. Although the Kohistan dunites could represent mantle melt channels that formed by melt-peridotite reactions (*17*) rather than the residues of partial melting, the results of such melt-rock reactions, i.e., the loss of pyroxene and the depletion of the rock in incompatible components, do not differ much from those produced by melt extraction. Spinels

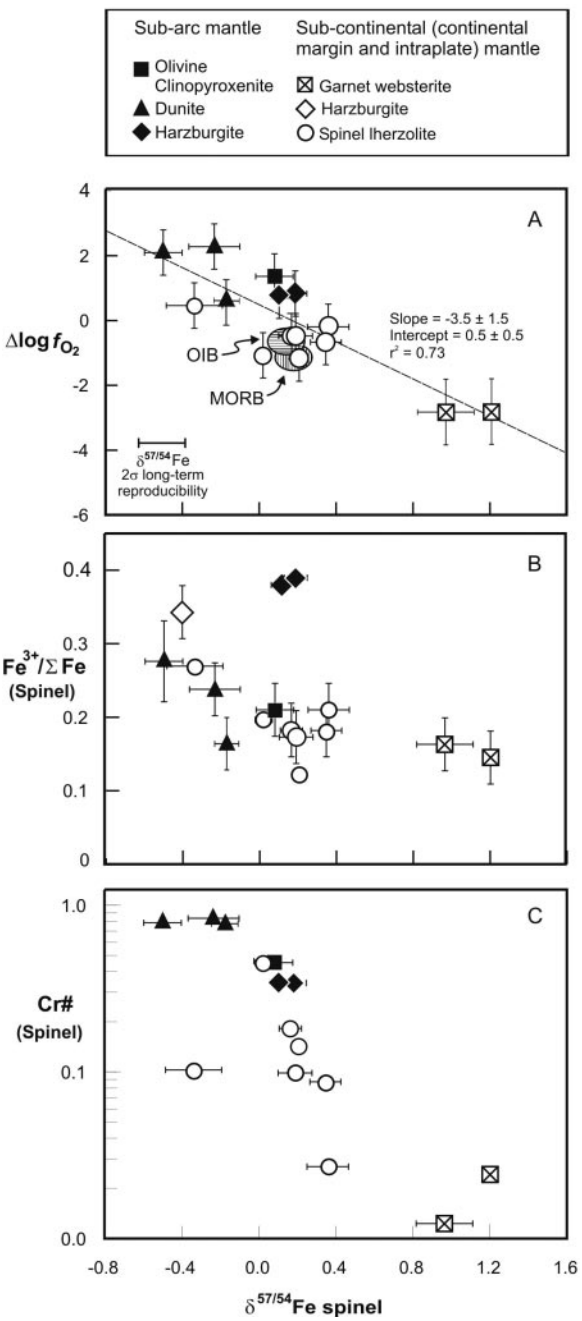

Fig. 1. (**A**) Spinel $\delta^{57/54}Fe$ (delta denotes the deviation of the measured isotopic composition from that of the IRMM-14 iron standard, expressed in parts per 1000), versus $\Delta\log f_{O_2}$. The errors on the spinel $\delta^{57/54}Fe$ values are given in Table 1. Errors of ±0.7 log-bar units were assigned to the $\Delta\log f_{O_2}$ values of the spinel-facies rocks, based on the sensitivity of the calculations to pressure and temperature and on the comparison of the different oxybarometers (*18*). The $\Delta\log f_{O_2}$ values plotted for the garnet websterites use the garnet $Fe^{3+}/\Sigma Fe$ ratios calculated from the trend of garnet $Fe^{3+}/\Sigma Fe$ with temperature (*18*) and have estimated errors of ±1.0 log-bar units, reflecting the maximum variation in $\Delta\log f_{O_2}$ obtained from different calculations of garnet $Fe^{3+}/\Sigma Fe$, the effects of temperature and pressure, and the use of combining data for different garnet grains within the sample (*18*). The shaded fields show the loci of the average MORB and OIB $\delta^{57/54}Fe$ (expressed relative to IRMM-14) and $\Delta\log f_{O_2}$ values (data sources in main text). (**B**) Spinel $\delta^{57/54}Fe$ versus spinel $Fe^{3+}/\Sigma Fe$ (errors in Table 1). (**C**) Spinel $\delta^{57/54}Fe$ versus $\log_{10}$ Cr number [molar Cr/(Cr+Al)].

that (re)crystallized in such rocks will share the same characteristics of residual spinels: high Cr number and $Fe^{3+}/\Sigma Fe$. In a slight modification of the melt extraction model described above, isotopically heavy iron could be preferentially extracted from the rock by the percolating melt, leaving an isotopically light and chemically depleted dunitic residue.

Intermineral iron isotope equilibration will also affect spinel $\delta^{57/54}Fe$ values, depending on sample mineralogy and the fractionation factors between different minerals. Available data for mantle peridotites (*3*) indicate that the variable modal proportions of silicate phases in these samples (*18*) are likely to have a much smaller effect on Fe isotope variations than the range observed for spinel and bulk rock $\delta^{57/54}Fe$ (1.7 and 0.9‰).

Spinels from garnet websterites display the heaviest $\delta^{57/54}Fe$ and lowest $\Delta\log f_{O_2}$ values. Websterites may represent cumulates that crystallized during basalt-peridotite interaction. In the case of P6 and P12, the cumulate phases are mainly low–ferric iron garnets and clinopyroxenes (*18*). The $\delta^{57/54}Fe$ and $\Delta\log f_{O_2}$ values of these samples can be explained if, during removal of intercumulus liquid, Fe^{3+} partitions preferentially into the liquid phase relative to garnet (*14*), driving the differentiated liquids to higher $\Delta\log f_{O_2}$ and leaving a reduced residue. This scenario reconciles the heavy $\delta^{57/54}Fe$ and $\Delta\log f_{O_2}$ values of P6 and P12 with the intermediate values of the spinel peridotites P13, C235A, and C271-I. The behavior of ferric iron during partial melting is likely to be very different in the spinel and garnet facies. In the garnet fa-

Table 1. Iron isotope and Mössbauer data, with calculated temperatures, pressures, and $\Delta\log f_{O_2}$ values. Abbreviations: Sp hz, spinel harzburgite; Ol cpx, olivine clinopyroxenite; Sp lhz, spinel lherzolite; Dun, dunite; Gt web, garnet websterite; USGS std, U.S. Geological Survey standard. n.d., not determined. Sample modal mineralogies are given as supporting online material (*18*).

Sample	Rock type	$\delta^{57/54}Fe$*	2σ†	$\delta^{57/56}Fe$	2σ	$Fe^{3+}/\Sigma Fe$‡	2σ	FeO§	Cr# §	*T* (°C) ol-sp‖	*T* (°C) 2-px‖	*T* (°C) opx‖	*P* (GPa)¶	$\Delta\log f_{O_2}$#
Spinels from the Jijal Complex, Kohistan Arc, Pakistan (fore-arc)														
J18/01	Dun	−0.50	0.10	−0.19	0.09	0.28	0.06	30.0	0.79	619		874	0.8	2.1
J27/01	Ol cpx	0.08	0.10	0.27	0.19	0.21	0.04	34.0	0.45	518	820	889	0.8	1.4
J30/01	Dun	−0.23	0.13	−0.13	0.27	0.24	0.04	29.5	0.83	576		607	0.6	2.3
Spinels from Simcoe, Washington, NW USA (fore-arc)														
SIM3	Sp hz	0.10	0.04	0.06	0.09	0.38	0.01	14.2	0.34	1035	938	931	0.7	0.8
SIM24	Sp hz	0.19	0.06	0.09	0.15	0.39	0.01	18.0	0.34	1098	984	976	0.2	0.8
Spinel from Twin Sisters, Washington, USA (fore-arc)														
TS-1	Dun	−0.17	0.06	0.01	0.32	0.16	0.04	18.0	0.78	752				0.6
Spinel from San Quentin, Baja Peninsula, Mexico (continental margin)														
BCN130	Sp lhz	−0.34	0.15	−0.10	0.26	0.27	n.d.	11.4	0.10	943	1040	1039	1.3	0.5
Spinels from Ventura-Espiritu, Santo, Mexico (continental margin)														
SLP114	Sp lhz	0.02	0.04	0.00	0.05	0.20	n.d.	14.0	0.46	903	1041	1033	0.4	−1.1
SLP403	Sp lhz	0.21	0.03	0.09	0.23	0.12	n.d.	10.5	0.14	686	1043	1067	1.4	−1.2
Spinel from Kilbourne Hole, New Mexico, USA														
KH96-2	Sp lhz	0.16	0.06	0.06	0.19	0.18	0.04	11.4	0.21	839	978	1016	0.5	−0.5
Spinels from Cameroon Line, transitional zone (continental margin)														
C235-A	Sp lhz	0.36	0.11	0.25	0.04	0.21	0.04	10.5	0.03	866		697	1.1	−0.2
C271-I	Sp lhz	0.19	0.09	0.09	0.15	0.17	0.04	9.8	0.10	920	923	973	1.3	−0.5
Spinels from Cameroon Line, continental (intraplate) zone														
P6	Gt wb	0.96	0.15	0.29	0.29	0.16	0.04	13.3	0.01		891	913	1.4	−2.9
P12	Gt wb	1.20	0.01	0.56	0.27	0.15	0.04	11.5	0.02		878	887	1.7	−2.9
P13	Sp lhz	0.35	0.08	0.12	0.11	0.18	0.04	10.8	0.09	837	692	688	1.4	−0.7
N12	Sp hz	−0.40	0.04	−0.11	0.09	0.34	0.04	n.d.	n.d.					
Bulk rock samples														
J18/01		−0.56	0.12	−0.23	0.18			12.1						
J27/01		0.16	0.10	0.20	0.24			5.90						
SLP403		0.02	0.09	−0.01	0.08			7.53						
KH96-2		0.06	0.01	−0.01	0.05			n.d.						
C271-I		0.10	0.05	0.10	0.20			8.35						
P6		0.32	0.10	0.00	0.07			8.14						
P12		0.37	0.02	0.09	0.09			n.d.						
BIR-1	USGS std	0.08	0.09	0.03	0.18			10.2						

*Each iron isotope analysis (quoted relative to IRMM-14) is the average of three to eight replicate analyses spread across different analytical sessions. †The errors quoted are the two standard deviations of the mean of the replicate sample analyses; in the case of J18/01 spinel, the average incorporates two separate sample dissolutions. The $\delta^{57/54}Fe$ composition that we measured for BIR-1 is given for comparison. ‡$Fe^{3+}/\Sigma Fe$ values were determined by Mössbauer spectroscopy for most samples except BCN-130, SLP114, and SLP403, for which they were calculated from electron microprobe data (*10*–*12*) by charge balance. §Total iron as FeO. Published electron microprobe data are presented for FeO (total) and Cr number [molar Cr/(Cr + Al)] contents of the Simcoe (*12*), San Quentin/Ventura-Espiritu (*10*), and Cameroon Line (*11*) samples. Electron microprobe data for the Kilbourne Hole, Twin Sisters, and Kohistan samples are available as supporting online material (*18*). ‖Temperatures given by the olivine-spinel (*8*), two pyroxene (*22*), and orthopyroxene (*23*) thermometers. ¶Pressures for spinel-facies rocks are calculated with the clinopyroxene-structure barometer (*24*); those for the samples P6 and P12 are taken from Lee *et al*. (*11*), where they were calculated using the garnet-orthopyroxene barometer (*25*). #Oxygen fugacity in log-bar units relative to the fayalite-magnetite-quartz (FMQ) buffer. The details of the thermobarometry and oxygen fugacity calculations are given as supporting online material (*18*). Although these parameters have been calculated previously for some of the samples (*10*–*12*), they are recalculated here to give a consistent data set.

cies, empirical observations suggest that ferric iron, predominantly hosted in garnet, behaves relatively incompatibly during melting, forming oxidized melts and reduced residues (*14*). In the spinel facies, ferric iron, principally accommodated in spinel, may behave more compatibly and be partly retained in the residue.

If heavy $\delta^{57/54}$Fe and $\Delta\log f_{O_2}$ values are generally applicable to garnet-facies melting residues, then a finite difference may exist between the $\delta^{57/54}$Fe and $\Delta\log f_{O_2}$ values of magmas produced by partial melting of garnet and spinel-facies mantle. However, oceanic island basalts (OIB) have only slightly higher $\Delta\log f_{O_2}$ (~ 0.8 log-bar units) values than mid-ocean ridge basalts (MORB) (*19*, *20*), and fractionally different average $\delta^{57/54}$Fe values (MORB, 0.18‰; OIB, 0.12‰) (*21*). OIBs may become oxidized relative to their source during melt segregation and decompression (*9*). If so, their more oxidized nature and lighter $\delta^{57/54}$Fe values may indicate that magma $\delta^{57/54}$Fe and $\Delta\log f_{O_2}$ values are coupled and controlled by melting regime and source mineralogy and do not directly reflect the $\delta^{57/54}$Fe and $\Delta\log f_{O_2}$ values of their source region. This limited variation in the $\Delta\log f_{O_2}$ values of MORB and OIB, compared to peridotites, may explain why previous studies of iron isotopes in mafic rocks, dominantly MORB and OIB (*21*), did not reveal large iron isotope variations.

Our results are readily explained if variations in spinel and bulk-rock $\delta^{57/54}$Fe are caused by melt-extraction processes accompanied by changes in mantle $\Delta\log f_{O_2}$. Although the $Fe^{3+}/\Sigma Fe$ of whole rocks and spinels can become decoupled from $\Delta\log f_{O_2}$ (*2*), the absence of outliers on the trend of $\delta^{57/54}$Fe and $\Delta\log f_{O_2}$ (Fig. 1A) suggests that iron isotopes in spinels are more resistant to resetting than spinel $Fe^{3+}/\Sigma Fe$. This is consistent with the observation that spinels from the metasomatized Simcoe xenoliths are displaced above the trend of $\delta^{57/54}$Fe with spinel $Fe^{3+}/\Sigma Fe$ (Fig. 1B), yet lie on the correlation between $\delta^{57}Fe/^{54}Fe$ and $\Delta\log f_{O_2}$. Hence, iron isotopes provide an independent means of estimating $\Delta\log f_{O_2}$ that can complement existing methods.

References and Notes

1. D. Canil, *Earth Planet. Sci. Lett.* **195**, 75 (2002).
2. J. W. Delano, *Orig. Life Evol. Biosph.* **31**, 311 (2001).
3. X. K. Zhu *et al.*, *Earth Planet. Sci. Lett.* **200**, 47 (2002).
4. V. B. Polyakov, S. D. Mineev, *Geochim. Cosmochim. Acta* **64**, 849 (2000).
5. E. A. Schauble, G. R. Rossman, H. P. Taylor Jr., *Geochim. Cosmochim. Acta* **65**, 2487 (2001).
6. H. S. O'Neill, V. J. Wall, *J. Petrol.* **28**, 1169 (1987).
7. B. J. Wood, L. T. Dryndzie, K. L. Johnson, *Science* **248**, 337 (1990).
8. C. Ballhaus, R. F. Berry, D. H. Green, *Contrib. Mineral. Petrol.* **107**, 27 (1991).
9. C. Ballhaus, *Contrib. Mineral. Petrol.* **114**, 331 (1993).
10. J. F. Luhr, J. J. Aranda-Gómez, *J. Petrol.* **38**, 1075 (1997).
11. D.-C. Lee *et al.*, *J. Petrol.* **37**, 415 (1996).
12. A. D. Brandon, D. S. Draper, *Geochim. Cosmochim. Acta* **60**, 1739 (1996).
13. I. J. Parkinson, R. J. Arculus, *Chem. Geol.* **160**, 409 (1999).
14. A. B. Woodland, M. Koch, *Earth Planet. Sci. Lett.* **214**, 295 (2003).
15. V. S. Kamenetsky, A. J. Crawford, S. Meffre, *J. Petrol.* **42**, 655 (2001).
16. R. J. Arculus, *Lithos* **33**, 189 (1994).
17. P. B. Kelemen, *J. Petrol.* **31**, 51 (1990).
18. Materials and methods are available as supporting material on *Science* Online.
19. A. Kiline, I. S. E. Carmichael, M. L. Rivers, R. O. Sack, *Contrib. Mineral. Petrol.* **83**, 136 (1983).
20. D. M. Christie, I. S. E. Carmichael, C. H. Langmuir, *Earth Planet. Sci. Lett.* **79**, 397 (1986).
21. B. L. Beard *et al.*, *Chem. Geol.* **195**, 87 (2003).
22. P. R. Wells, *Contrib. Mineral. Petrol.* **62**, 129 (1977).
23. J.-C. C. Mercier, *Tectonophysics* **70**, 1 (1980).
24. P. Nimis, P. Ulmer, *Contrib. Mineral. Petrol.* **133**, 122 (1998).
25. G. P. Brey, T. Kohler, *J. Petrol.* **31**, 1353 (1990).

26. This paper benefited from discussions with J. Connolly, D. Harrison, T. Holland, R. Kessell, S. Nielsen, I. Parkinson, R. Powell, U. Wiechert, and P. Ulmer. O. Jagoutz provided invaluable help in collecting the Kohistan samples. We thank D. Barford, A. Brandon, D.-C. Lee, J. Luhr, and M. Rekhämper for providing additional samples. We also thank C. Stirling, F. Oberli, and U. Menet for technical help. This project was supported by ETH Zürich and the Swiss National Fonds (grant 20-61465.00 to J.-P. B.).

Supporting Online Material

www.sciencemag.org/cgi/content/full/304/5677/1656/DC1
Materials and Methods
Tables S1 and S2
References

15 January 2004; accepted 6 May 2004

New Zealand Maritime Glaciation: Millennial-Scale Southern Climate Change Since 3.9 Ma

Robert M. Carter* and Paul Gammon

Ocean Drilling Program Site 1119 is ideally located to intercept discharges of sediment from the mid-latitude glaciers of the New Zealand Southern Alps. The natural gamma ray signal from the site's sediment core contains a history of the South Island mountain ice cap since 3.9 million years ago (Ma). The younger record, to 0.37 Ma, resembles the climatic history of Antarctica as manifested by the Vostok ice core. Beyond, and back to the late Pliocene, the record may serve as a proxy for both mid-latitude and Antarctic polar plateau air temperature. The gamma ray signal, which is atmospheric, also resembles the ocean climate history represented by oxygen isotope time series.

Recent comparisons between climate proxies from subpolar sediment cores and polar ice cores suggest that Southern Hemisphere events lead those from the north by ~1.5 to 3 thousand years (ky) (*1*–*3*). In reality, two geographical data points located near opposing poles are inadequate to allow such a unique causality and time lag to be inferred (*4*). A better understanding of climate dynamics with respect to the coupling of the Northern and Southern Hemispheres therefore requires the assembly of additional climate records across the critical mid-latitude temperate zones. Here we present a 3.9 million year (My)–long record of glaciation in the New Zealand Southern Alps, as preserved in a core through intermediate water-depth sediment drifts from Ocean Drilling Program (ODP) Site 1119, east of South Island, in the southwest Pacific Ocean (Fig. 1).

The New Zealand Southern Alps are a 600-km-long chain of mountains that today host more than 3000 glaciers individually larger than 0.01 km^2, with a total area of 1159 km^2 and a combined ice volume of 53 km^3 (*5*). Temperate maritime glaciers are particularly sensitive to climate perturbations because of their high accumulation and ablation rates (*6*). The mid-latitude location of the Southern Alps, at the junction between subtropical and polar air masses and near major ocean fronts such as the Subtropical Front (STF), adds even more to their sensitivity as a monitor of climatic change.

It is currently controversial whether recent climate fluctuations from mid-latitude New Zealand relate primarily to Northern or Southern Hemisphere polar records (*7*–*10*). The Site 1119 record, when compared at millennial resolution with that of the Vostok ice core, shows that New Zealand climate cyclicity resembles that of Antarctica back to at least Marine Isotope Stage (MIS) 11, ~0.37 million years ago (Ma) (*11*). This level corresponds to the present base of the Antarctic ice core record. Beyond it, the cyclicity in the 1119 core records a changing mid-latitude ice signal that may continue to serve as a proxy for Antarctic polar plateau air

School of Earth and Environmental Sciences, University of Adelaide, Adelaide, SA 5005, Australia.

*To whom correspondence should be addressed. E-mail: bob.carter@jcu.edu.au